Piezocatalytic activity of CaO–Bi$_2$O$_3$–B$_2$O$_3$ glass-ceramics under ultrasonic vibrations

Chirag Porwal ; Vishal Singh Chauhan ; Rahul Vaish

Check for updates

View Online

Export Citation

Piezocatalytic activity of CaO–Bi₂O₃–B₂O₃ glass-ceramics under ultrasonic vibrations

View Online   Export Citation   CrossMark

Chirag Porwal, [iD] Vishal Singh Chauhan,[a] [iD] and Rahul Vaish[a] [iD]

AFFILIATIONS

School of Mechanical and Materials Engineering, Indian Institute of Technology, Mandi, Himachal Pradesh 175005, India

[a]Authors to whom correspondence should be addressed: vsc@iitmandi.ac.in and rahul@iitmandi.ac.in

ABSTRACT

Transparent glass-ceramics of CaO–Bi₂O₃–B₂O₃ (CBBO) were fabricated using the conventional melt quench technique. X-ray diffraction and Raman spectroscopy were employed to confirm the phase of the prepared samples. Differential scanning calorimetry (DSC) was used to verify that the material was, indeed, glassy. The CBBO glass samples were subjected to heat treatment at 540 °C for 30 min and 1 h based on their crystallization temperature obtained from DSC analysis. This study focused on the piezocatalytic behavior of CBBO glass-ceramic samples. Piezocatalysis experiments were conducted on the fabricated glass-ceramic samples, and it was discovered that the samples heat-treated for 30 min (HT30m) at 540 °C showed maximum dye degradation of 61% under 240 min of ultrasonication. Experiments were repeated multiple times to confirm their reliability. Additionally, a phytotoxicity assessment was performed on the degraded dye using vigna radiata seeds. The antibacterial properties of the CBBO glass-ceramic samples were also investigated via piezocatalysis. It was discovered that the HT30m CBBO glass-ceramic sample removes 98% of *Escherichia coli* and 99% of *Staphylococcus aureus* bacteria within 120 min of ultrasonication.

I. INTRODUCTION

Glass-ceramics are a unique class of materials due to several merits such as ease of manufacturing, low cost, tunable microstructure, and stable mechanical, chemical, and thermal properties.[1,2] Hence, glass-ceramics have been used in a wide range of applications. Several glass-ceramics are now trademarks of products such as Zerodur, Gorilla Glass, and 45S5 Bioglass.[3] In further exploring the horizon of glass-ceramics in the sustainable growth of society, glass-ceramics can be re-looked at for environmental remediation applications. The environment is constantly being threatened by various contaminants present in the water, soil, and air.[4,5] These contaminants comprise fatal chemicals and, due to the risks they threaten to an ecosystem, will directly or indirectly affect human health.[6] As always, clean water, clean soil, and clean air are key components to sustain life on Earth, so the remediation of polluted environments is an immediate necessity. Water cleaning is one of the global challenges and needs the attention of researchers. Various materials have shown water-cleaning possibilities in view of adsorption, photocatalysis, and antibacterial characteristics.[7] For instance, TiO₂ is widely known for its photocatalytic activity.[8] Furthermore, ferroelectric ceramics have shown better performance in view of photocatalysis due to the associated internal electric field. The internal electric field supports the separation of electrons and holes for a long time and provides a longer duration of catalytic reactions.[9] Materials such as BaTiO₃, LiNbO₃, and Ba₀.₅Sr₀.₅TiO₃ are well explored.[10–13] Recently, ferroelectric glass-ceramics have also been reported for photocatalytic applications.[14–17] Ferroelectric materials are known for their piezoelectric and pyroelectric properties. Electromechanical and electrothermal coupling allows sensing and energy harvesting possibilities. These properties are widely explored in single crystals, polycrystalline ceramics, polymer composites, etc. However, ferroelectric glass-ceramics have not shown any promising sensing and energy harvesting application due to very weak coupling. Piezocatalysis is one of the couplings where mechanical vibrations can trigger an electric field followed by catalysis.[18] As catalysis requires less input energy, ferroelectric glass-ceramics may show some promising signals irrespective of very weak coupling. The present study is planned to explore such possibilities. Glass-ceramics are a suitable candidate for

water-cleaning applications via piezocatalysis.[19] Some recent studies have reported glass-ceramics as a catalyst for water-cleaning applications via piezocatalysis.[20,21]

CaBi$_2$B$_2$O$_7$ (CBBO) fabricated via a solid-state reaction route has recently been explored and reported for its non-centrosymmetric structure, which is essential for piezocatalytic activity.[22] Due to the presence of borate (a good glass former), the above-mentioned composition can be melted at a lower temperature and CBBO is expected to quench into glasses at a moderate temperature range. Glass-ceramics containing non-centrosymmetric crystals within the glass matrix can demonstrate piezocatalysis. The present study focuses on the use of CaBi$_2$B$_2$O$_7$ (CBBO) glass-ceramics for piezocatalysis applications.

II. EXPERIMENTAL

CaO–Bi$_2$O$_3$–B$_2$O$_3$ (CBBO) transparent glasses were prepared through the conventional melt quench technique. High-purity reagents (>99%) of CaCO$_3$, H$_3$BO$_3$, and Bi$_2$O$_3$ were taken in their stoichiometric ratios for the fabrication of CBBO glasses. The powders of the primary precursors were appropriately mashed in a mortar and pestle to ensure compositional homogeneity, and afterward, the powder mix was poured into a platinum crucible. The crucible with the prepared powder is placed in an electric furnace (Nabertherm, Germany). The temperature of the furnace is set at 1000 °C. The crucible was subjected to an established temperature for 10 min. The crucible was taken out from the furnace, and the melt was poured onto a stainless-steel plate to quench the glass. The plate was preheated to 300 °C and then compressed with a second plate heated to 300 °C. The process of quenching glass is shown in Fig. 1.

Annealing of the prepared glass was done at 350 °C for 5 h. The crystallization of the samples was accomplished by heat treatment to the transparent yellow CBBO glass plate for various time durations. Differential scanning calorimetry (DSC) was performed (with Perkin Elmer, STA-6000 instrument) in the range of 350–600 °C at a heating rate of 10 °C/min in a nitrogen environment to assess the temperature and time duration of the heat treatment. In accordance with the DSC, samples were heated to 540 °C for 30 min and 1 h for crystallization. X-ray diffraction (XRD) was performed on the as-quenched (AQ) and heat-treated samples of CBBO glass plates to confirm their amorphous and crystalline nature. X-ray diffraction analysis was performed using a Rigaku (Japan) powder diffractometer with a 9 kW rotating anode made of Cu Kα. The XRD experimental was performed in the range of 10°–70° 2θ range with a scanning speed of 2°/min for the identification of the present phase in CBBO glass and glass-ceramic samples under consideration. After getting confirmation regarding phase, Raman spectroscopy was performed

to get knowledge about various vibration modes using HORIBA (Model-lab RAM HR Evolution) for the fabricated samples of CBBO glass and glass-ceramics (AQ, HT30m, and HT1h). To examine the surface morphology of the samples, field emission-scanning electron microscopy (FE-SEM, NOVA NANO SEM-450) was utilized. X-ray photoemission spectroscopy (XPS) was used to study the oxygen states in the form of non-binding and binding oxygen by O1s scans of samples under consideration. The spectra were recorded using an Al-Kα source and a Nexsa x-ray photoemission spectrophotometer.

The degradation of methylene blue (MB) dye as a model dye via piezocatalysis was carried out using the fabricated CBBO glass-ceramic samples. The initial concentration of the dye was considered as 5 ppm (5 mg/l concentration). The presence of a pollutant in water was quantified as a dye, which was collected into separate glass beakers with samples of AQ, HT30m, and HT1h in their 140 mm^2 surface area for conducting piezocatalysis experiments. As a first step, each sample was immersed in the beaker containing the dye (5 ml of 5 mg/l concentration) for 4 h and placed in the dark, away from any other light source, to avoid deterioration until adsorption–desorption equilibrium was reached. To create mechanical vibrations, the beaker containing the samples and the dye was put in an ultrasonicator operating at 150 W power and 40 kHz frequency. Water was used as a medium to transport induced vibrations from the sonicator to the sample, and its temperature was kept below 15 °C during the tests. To rule out the possibility of any other catalytic mechanism contributing to the degradation of dye, all piezocatalysis studies were carried out in the dark. Dye deterioration was determined using a Shimadzu UV-2600 UV–visible spectrophotometer. A total of 4 h was devoted to each experiment, with 1 ml of aqueous dye solution being removed and measured every 30 min. The recovered dye solution was then added back to the original dye solution to maintain the same volume throughout the experiment. Using Eq. (1), we were able to determine the percent of dye degradation, where the concentration of dyes is at t = 0 and t = t$_{min}$, respectively,

$$Degradation~of~dye(\%) = \left(1 - \frac{Final~concentration~of~dye}{Initial~concentration~of~dye}\right)*100. \tag{1}$$

The effect of the antibacterial treatment on *Escherichia coli* (*E. coli*, gram-negative) and *Staphylococcus aureus* (*S. aureus*, gram-positive) was investigated via piezocatalysis while maintaining the same experimental condition as the degradation of dye in the ultrasonicator by using the fabricated CBBO glass-ceramic samples. For plating agar, a Mueller–Hinton agar plate mix was used. The preparation of bacterial cells was done by growing them overnight in
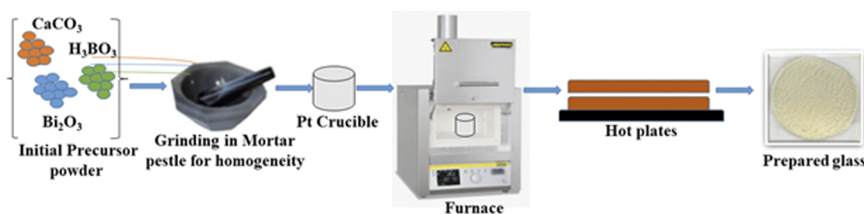

FIG. 1. Process flowchart for the preparation of CBBO glasses.

the Luria–Bertani (LB) broth medium at 180 rpm with a temperature of 37 °C from *E. coli* and *S. aureus*. Cultured plates of agar, carrying the prepared bacteria of *E. coli* and *S. aureus*, were subjected to ultrasonication in the presence and absence of an HT30m CBBO glass-ceramic sample. Using the solidified agar plate colony counting method with serial dilutions of phosphate-buffered saline (PBS), we found that the CFUs/ml of *E. coli* and *S. aureus* in the working suspension were 95×10^6 and 103×10^7, respectively. 1.5 ml of the prepared bacterial suspension was placed in a glass vial with (70×70 mm^2) of AQ and HT30m samples of the CBBO glass-ceramic immersed in the suspension of bacteria. After the piezocatalytic experiments were conducted on the prepared solutions, the desired dilution was achieved, from which 100 μl of solution is taken in desired time intervals and spread onto the prepared agar plates. The obtained solution of 100 μl was cautiously distributed on the agar plate to determine the logarithmic decrease in bacteria. The following equation is used for calculating the same:

$$Log\ reduction = \log_{10}\left(\frac{N_0}{N}\right) = \log_{10}N_0 - \log_{10}N, \qquad (2)$$

where N_0 = the count of CFUs/ml in the bacterial solution at time t = 0 min and N = the count of CFUs/ml in the bacterial solution at time t min, during piezocatalysis experiments.

III. RESULTS AND DISCUSSION

Differential scanning calorimetry (DSC) was performed on the as-quenched sample of the CBBO glass plate to determine the glass transition (T_g), the onset of the crystallization (T_{cr}), and the peak crystallization (T_p) temperatures. The obtained trace of DSC for the CBBO glass plate is shown in Fig. 2. The DSC curve represents the glass transition temperature, and the exothermic peak represents the crystallization of the glass plate as a function of temperature. The nucleation and development of crystals in the CBBO glass plate are responsible for the transition from the glassy to the crystalline phase. It is well established that the method of crystallization affects the formation of exothermic peaks, with sharp and broad peaks corresponding to the surface and bulk crystallization, respectively. The obtained broad peak of the exotherms shows the dominance of surface crystallization.
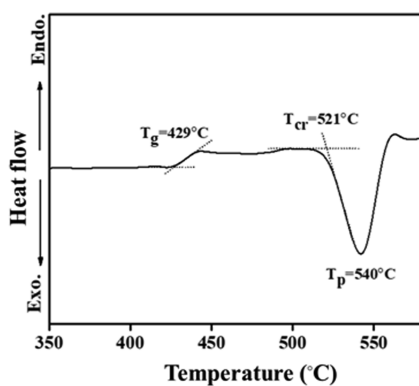
The glass transition temperature (T_g) and the onset of the crystallization temperature (T_{cr}) are found to be 429 and 521 °C. The difference between T_g and T_{cr} can be understood in terms of the thermal stability of the fabricated CBBO glasses. Generally, the thermal stability is the parameter that is studied to estimate the stability of glasses given by ΔT. To calculate the thermal stability, Eq. (3) can be used as follows:[23]

$$\Delta T = T_{cr} - T_g. \qquad (3)$$

The higher difference between the glass transition (T_g) and the onset of crystallization (T_{cr}) will lead to the better stability of the glasses. To study the thermal stability of the glasses, Saad and Poulin gave a parameter to study the resistance to devitrification of the glasses given by S as shown in Eq. (4),[24]

$$S = \frac{(T_p - T_{cr})(T_{cr} - T_g)}{T_g}, \qquad (4)$$

where ($T_p - T_{cr}$) shows the rate of devitrification transformation of the glassy phases. For the present glass sample of CBBO, the calculated value for S is 4.07, which is higher than the Bi_2O_3–B_2O_3 (3.07) based glasses, indicating a better thermal stability.[25]

X-ray diffraction (XRD) was performed and plotted (Fig. 3) for the as-quenched (AQ) glass with the heat-treated samples of the CBBO glass-ceramic plate. The obtained plots of XRD clearly show the transformation from the glassy phase of the AQ glass plate to the crystalline phase of the heat-treated glass-ceramic samples. As the duration of heat treatment is varied from 30 min to 1 h, the glass sample transformation is observed as the glass converts into a glass-ceramic. The glass-ceramic under investigation indicated the crystallization with planes (113) and (020) for the 30-min heat-treated sample and with planes (002), (011), (111), (113), (210), (013), (020), (310), (312), (221), and (400) for the 1-h heat-treated sample in orthorhombic phase. These observed planes are in good agreement with the polycrystalline CBBO, as it is confirmed that the transformation of the amorphous phase to the crystalline phase of glass under consideration can be achieved by the heat-treatment process.[22]

Raman spectroscopy in the range of 100–1200 cm^{-1} was performed at room temperature for the prepared CBBO glass and
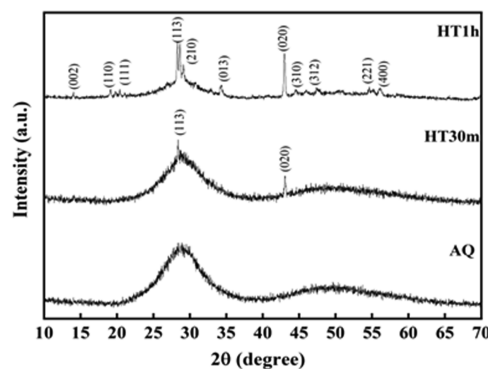
FIG. 2. DSC plot for the CBBO glass plate.

FIG. 3. XRD plots of the AQ, 30-min heat-treated (HT30m), and 1-h heat-treated (HT1h) glass samples at 540 °C.
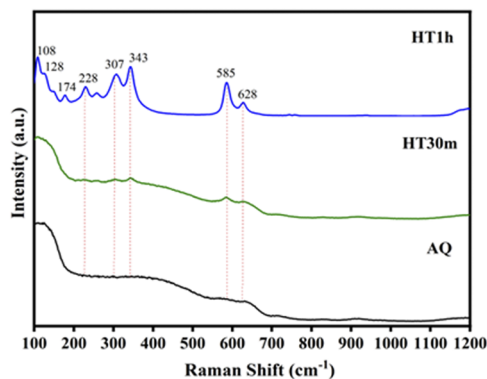
18 April 2024 20:02:34

FIG. 4. Raman spectra of the CBBO glass and glass-ceramic samples.

glass-ceramic samples. The material under consideration $CaBi_2B_2O_7$ (CBBO) in the orthorhombic space group is a novel structure type belonging to $CaBi_2O(BO_3)_2$.[26] The crystal structure of the CBBO is an arrangement of layers built of corner-sharing BO_3 in a triangular form and CaO_6 in a trigonal prism with Bi_2O groups accommodated within six-membered rings. For the crystal lattice of CBBO, four formula units per primitive cell are there. The layers of BO_3 triangles held together by O–Bi–O bridges are the common motif in the case of $CaBi_2B_2O_7$. The Raman active modes of samples under investigation can be classified into two categories as a low-frequency group (<350 cm^{-1}) and a high-frequency group (>350 cm^{-1}). The responsible compound for the low-frequency vibration modes is Bi–O polyhedral, while the high-frequency spectra are dominated by B–O triangles.[27] The observed spectra of the AQ, HT30m, and HT1h samples of the CBBO glass-ceramic plate are shown in Fig. 4. The transformation of the amorphous phase to the crystalline phase in the heat-treated samples can be observed as the broadening and sharpening of the peaks, which is also confirmed by the XRD. The observed peaks at 108, 128, 174, 228, 307, and 343 cm^{-1} are due to the heavy metal ion vibrational modes and vibrational modes in the borate framework. The modes observed at 585 and 628 cm^{-1} are due to the bending vibration state of $(BO_3)^{3-}$.[28]

Scanning electron microscopy (SEM) was performed, and images were collected for the CBBO glass and glass-ceramic samples as shown in Fig. 5. Figure 5(a) corresponds to the as-quenched glass sample, and it has been observed that there are no crystals present

on the surface of the sample confirming the glassy nature. The optical image of the sample is also shown (inset) with SEM micrographs indicating the physical appearance of the sample as a transparent glass. Figure 5(b) shows the SEM micrograph of the 30 min heat-treated glass-ceramic sample at 540 °C, confirming the formation of crystals on the surface of the glass-ceramic sample. Figure 5(c) shows the morphology of a 1-h heat-treated sample at 540 °C with its optical image (inset). It has been observed that the glass is transformed into a glass ceramic.

X-ray photoelectron microscopy (XPS) was utilized to identify the surface chemical state and chemical composition of the CBBO glass and glass-ceramic samples. Figure 6 shows the obtained spectra, in which Fig. 6(a) is the survey representing the presence of the elements in CBBO glass. The changes in the oxygen state of the AQ, HT30m, and HT1h CBBO glass-ceramic samples are shown in Figs. 6(b)–6(d). Oxygen concentration in a sample can be measured in terms of bridging sites (BO) and non-bridging sites (NBO).[29] According to the crystal structure of glass under consideration, the bridging sites are occupied by the two units of BiO_4 connected by the covalent bond of Bi–O–Bi and the non-bridging sites are the result of network modifiers mixed in the glass matrix, such as Ca^{+2}.[30] It has been found that the effect of network modifiers due to the crystallization of CBBO glass-ceramic by heat treatment in the glass matrix increases NBO and decreases BO, which is shown by the O1s spectra of the AQ, HT30m, and HT1h heat-treated samples.[31] The splitting of peaks in the O1s spectra of the heat-treated samples can be seen as shown in Figs. 6(c) and 6(d) having two peaks at 529.12 and 530.78 eV for HT30m and at 529.9 and 532 eV for HT1h CBBO glass-ceramic sample, which correspond to non-bridging sites and bridge sites.

The fabricated CBBO glass-ceramic samples were used to get the absorbance spectra from the UV–visible spectroscopy in the range of 200–800 nm of wavelength. The observed spectra are shown in Fig. 7(a), and it has been discovered that as glass is crystallized into glass-ceramic samples, the absorbance rises, while the transparency falls. The transparency of the prepared glass-ceramic samples of CBBO is acquired with UV–visible spectroscopy, and it was found that the AQ glass sample of CBBO has a transparency of 72% and HT30m has 68% transparency, respectively, also plotted and shown in Fig. 7(b). There is no denying that the crystallization reduces transparency. The HT1h sample is transformed into a glass-ceramic after the crystallization takes place with zero transparency, which can be confirmed by the digital images shown in Fig. 5 (inset).
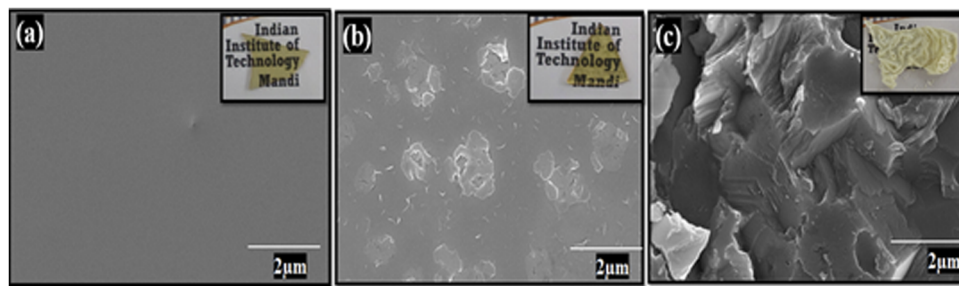

FIG. 5. SEM images of the (a) as-prepared (AQ), (b) HT30m, and (c) HT1h samples. The insets show optical images.
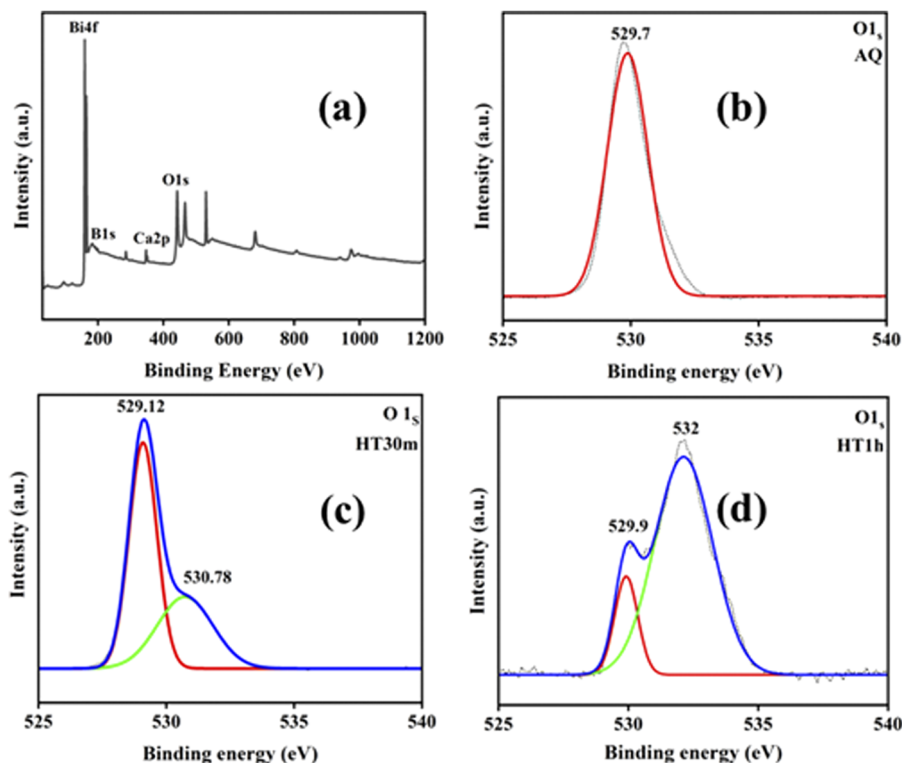
FIG. 6. XPS: (a) survey, (b) O1s spectrum (AQ glass), (c) O1s spectrum (HT30m glass-ceramic), and (d) O1s spectrum (HT1h glass-ceramic) samples.
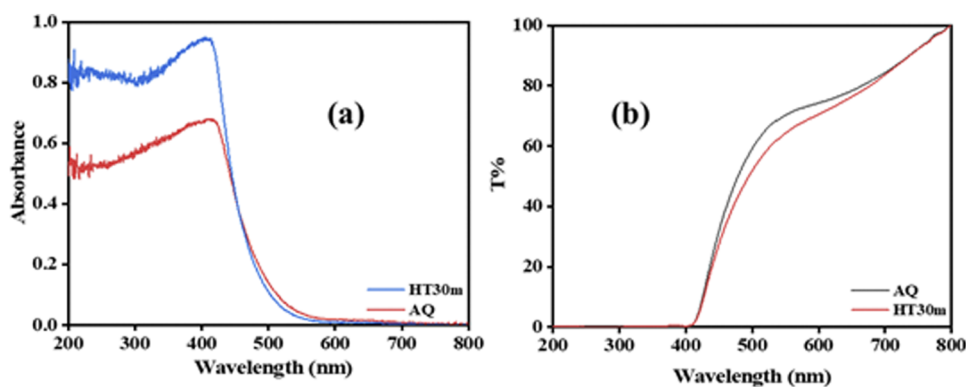

FIG. 7. (a) Absorbance plot and (b) transparency results of the CBBO glass-ceramic samples.

The elimination of pollutants from the organic dye (MB) is done via piezocatalysis with the fabricated CBBO glass-ceramic samples. Dye degradation results with AQ, HT30m, and HT1h with the degradation of the control MB dye are shown in Fig. 8. The sample with the highest level of dye degradation under consideration is HT30m, and its reduction in peak intensity while performing piezocatalysis every 30-min up to 240 min is shown in Fig. 8(a). The obtained result indicates the capabilities of the CBBO glass-ceramic sample for dye degradation using ultrasonication. Figure 8(b) shows the capabilities as a catalytic material for dye degradation of samples under consideration in the form of C/C_0 to time. The obtained result for dye degradation of the control MB dye is 12%, and the dye degradation with AQ, HT30m, and HT1h CBBO glass-ceramic samples is 20%, 68%, and 50%, respectively, under the action of ultrasonication for 240 min, as shown in Fig. 8(d). The sample heat-treated for 30 min (HT30m) at 540 °C shows the maximum degradation of MB dye. In this regard, it is worth noting that a larger surface area is crucial for catalytic activity. Since the specific surface area of a smaller crystal is bigger, more catalytic sites can be occupied by the crystal. When the heat treatment temperature or time is increased, more
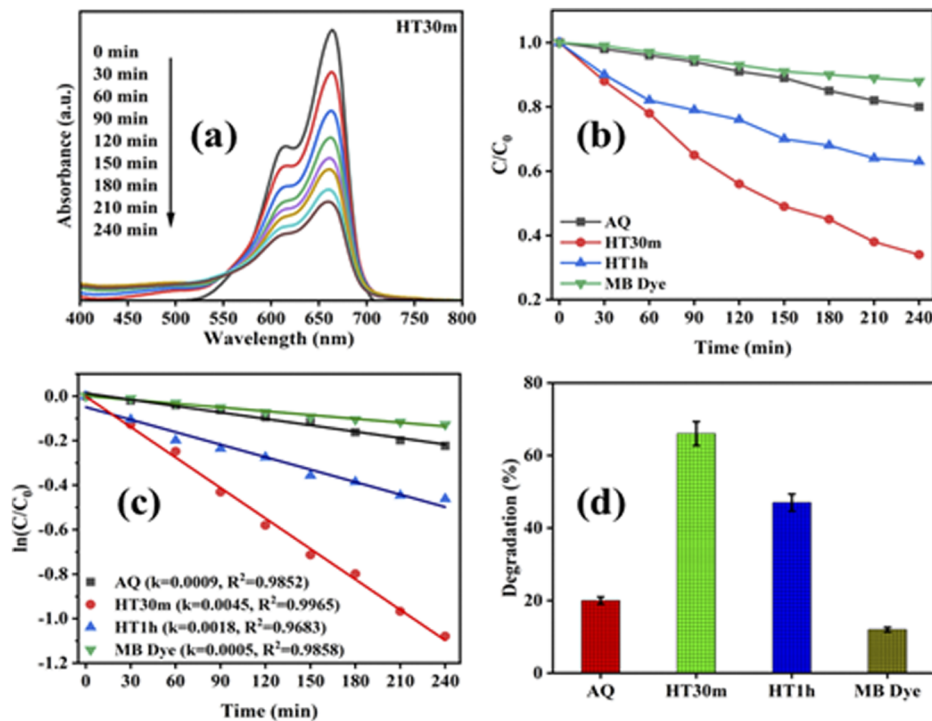
18 April 2024 20:02:34

FIG. 8. (a) Absorbance spectra of the HT30m CBBO glass-ceramic. [(b) and (c)] Results for kinetic rate. (d) Obtained degradation with samples under consideration.

crystals form, which might decrease the material's catalytic activity. Figure 8 depicts a similar pattern, which can be seen here. The first-order kinetics describes the decay [Eq. (5)],[32]

$$\ln\left(\frac{C}{C_0}\right) = -kt, \tag{5}$$

where

C = the dye concentration at time t;
C_0 = the dye concentration at time t_0; and
k = the rate constant.

Using CBBO glass-ceramic samples, we determined the degradation rate constants (k), calculated as shown in Fig. 8(c). 0.0005, 0.0009, 0.0045 and 0.0018 min^{-1} are the obtained slopes for the control MB dye, AQ, HT30m, and HT1h glass-ceramic sample of CBBO, respectively. Among the prepared glass-ceramic samples, HT30m

showed the highest dye degrading capability, with the highest k value of 0.0045 min^{-1}. It is because the HT30m sample has a lower crystalline size, which contributes to a higher specific surface area. With the increase in temperature/time of heat treatment, the crystal grows and the specific surface area decreases.

To understand more about the mechanism involved in piezocatalysis dye degradation using the CBBO glass-ceramic samples, a scavenger test is carried out. The maximum efficient CBBO glass-ceramic sample heat-treated at 540 °C for 30 min (HT30m) is used for radical tapping (Scavenger) experiments by degrading MB. Ethylenediaminetetraacetic acid (EDTA), isopropanol (IPA), and *p*-benzoquinone (BQ) were used to mitigate the holes (h+), hydroxyl radicals (˙OH), and superoxide radicals (˙O2) generated during piezocatalysis.[33,34] The obtained results for the scavenger test, as shown in Fig. 9(a), indicate that EDTA more significantly inhibits degradation as compared to BQ and IPA, which shows the
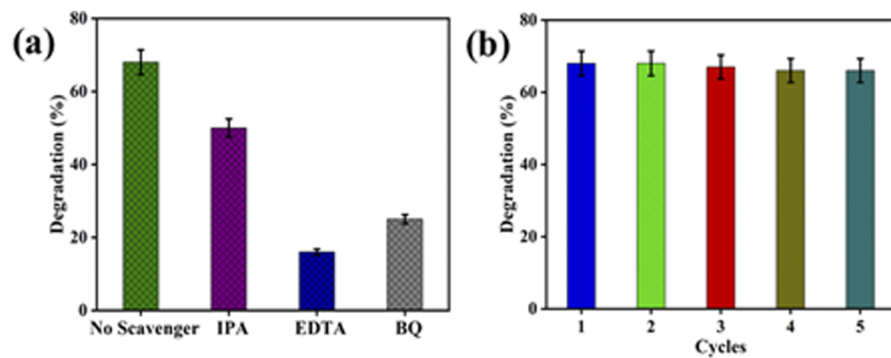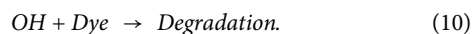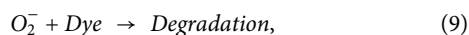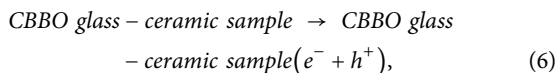

FIG. 9. (a) Scavenger results; (b) repeatability test.

18 April 2024 20:02:34

involvement of primary reactive species h^+ in the degradation process via piezocatalysis. Experiments for piezocatalysis dye degradation were performed several times using the prepared CBBO glass-ceramic samples to check the reliability, as shown in Fig. 9(b). To our knowledge, no massive changes occurred in the obtained data. Thus, the CBBO glass ceramic is a good candidate for piezocatalysis.

The removal of organic pollutants from water is carried out with the MB dye. Ultrasonication of water is used for conducting experiments that result in the formation of bubbles, followed by bubble growth and, then ultimately, collapse. The continuous cycle of this bubble formation, growth, and collapse results in the generation of high-temperature regions of around 5000 K with a high-pressure wave of 10^8 Pa. Because of this high temperature and pressure, the bubble decomposes into the radical species that will combine with the dye and take part in the degradation process via sonolysis (thermolysis).[35,36] It is expected that sonocatalysis is equally influenced in the as-quenched and heat-treated samples. As can be seen from the results, there are almost negligible dye degradation values for the heat-treated samples. The degradation of dye without any sample with ultrasonication resulted in 12% of degradation in 240 min by thermolysis. However, the samples of the CBBO glass-ceramic contribute to dye degradation via piezocatalysis. The generation of piezoelectricity by the CBBO glass-ceramic samples during ultrasonication results in the separation of charges via electrochemistry, which leads to dye degradation by redox reactions. A hypothetical mechanism that involves dye degradation by piezocatalysis can be understood as[37]

$$CBBO\ glass - ceramic\ sample\ \rightarrow\ CBBO\ glass - ceramic\ sample(e^- + h^+), \tag{6}$$

$$e^- + O_2 \rightarrow O_2^-, \tag{7}$$

$$h^+ + OH^- \rightarrow OH, \tag{8}$$

$$O_2^- + Dye \rightarrow Degradation, \tag{9}$$

$$OH + Dye \rightarrow Degradation. \tag{10}$$

When the crystallite of the CBBO glass-ceramic samples was strained by vibrations provided with ultrasonication, an electric field is generated. Due to this, localized electric field generation of polar surface takes place, as one is negative and the other is positive. The influence of this localized electric field leads to the movement of separated charges in the CBBO crystallites toward the surfaces ($e^- \rightarrow$ positive surface and $h^+ \rightarrow$ negative surface), respectively, and participates in the generation of free radicals. On the positive surface, the free-electron will be captured and the dissolved oxygen will be reduced to give superoxide anions; at the negative surface, protons will combine with hydroxyl ions to give hydroxyl radicals. These generated ·OH and ·O_2^- act as strong oxidants, which will attack dye molecules leading to the degradation of dye as a result. Some of the previously reported borate-based materials for catalytic applications are summarized and compared to our present study in Table I.

TABLE I. Borate-based materials with process parameters for different catalytic applications.

| Material	Material physical form	Catalytic dosage	Detection molecule	Degradation mechanism	Activity observed (%)	Power source	Reference
$InBO_3$	Powder	0.325 mg/ml	Chlorophenol	Photo-catalysis	92	UV-light, $\lambda > 30$ nm	38
YBO_3	Powder	3.33 mg/ml	Rhodamine B	Photo-catalysis	90	UV-light, $\lambda > 250$ nm	39
$Bi_4B_2O_9$	Powder	0.5 mg/ml	Methylene blue	Photo-catalysis	88	Solar light	40
$Zn_4B_6O_{13}$	Powder	1.6 mg/ml	Tetracycline solution	Photo-catalysis	80	UV-light	41
$Bi_2ZnOB_2O_6$	Powder	3.33 mg/ml	Rhodamine B	Photo-catalysis	98	UV-light, $\lambda > 250$ nm	42
$Na_3VO_2B_6O_1$	Powder	1 mg/ml	Chlorophenol	Photo-catalysis	82	Visible light	43
$NaZnB_5O_{10}$	Powder	0.5 mg/ml	Chlorophenol	Photo-catalysis	68	UV-light	44
$KZnB_5O_{10}$	Powder	0.5 mg/ml	Chlorophenol	Photo-catalysis	75	UV-light	44
$WO_3–ZnO–B_2O_3$	Glass-ceramic	1 mg/ml	Methylene blue	Photo-catalysis	95	UV-light, $\lambda = 254$ nm	14
$SrO–Bi_2O_3–B_2O_3$	Glass-ceramic	10 mm²/ml	Methylene blue	Photo-catalysis	70	UV-light, $\lambda = 365$ nm	15
$Bi_2ZnOB_2O_7$	Glass nanocomposite	28 mm²/ml	Methylene blue	Piezocatalysis	78	Ultrasonicator, 150 W, 40 kHz	45
$SrO–Bi_2O_3–B_2O_3$	Glass-ceramic	32 mm²/ml	Methylene blue	Piezocatalysis	51	Ultrasonicator, 150 W, 40 kHz	46
CBBO ($CaO–Bi_2O_3–B_2O_3$)	Glass-ceramic	28 mm²/ml	Methylene blue	Piezocatalysis	68	Ultrasonicator, 150 W, 40 kHz	The present study

18 April 2024 20:02:34
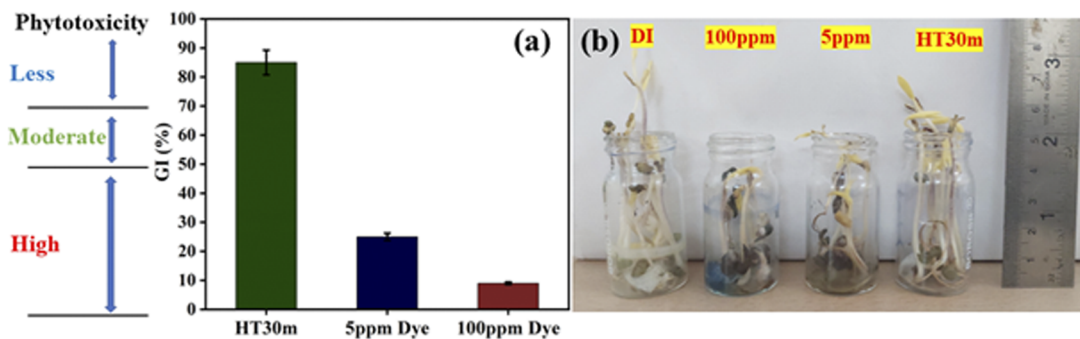
FIG. 10. (a) GI for phytotoxicity of 5, 100 ppm, and the water treated using HT30m samples and (b) vials containing seed germination after 7 days with control sample and other samples under consideration.

The presence of untreated effluent in irrigation water bodies is extremely harmful to the environment, and it affects ecosystem safety. Irrigation water is one of the crucial components that affect soil fertility. As the biodegradation of effluent products takes place, a variety of byproducts emerge, so an investigation of the toxicity of these byproducts on plants needs to be done. The presence of high protein and nutrients in the sprouted vigna radiata seeds is the reason why it is consumed all over the world. To find out the toxicity of polluted water treated with the CBBO glass-ceramic samples, the relative sensitivity of vigna radiata seeds toward the MB dye and its byproducts has been studied. Germination of vigna radiata seeds in deionized water is taken as a control sample with 100% germination. The results after 7 days of seed germination are plotted as shown in Fig. 10. As shown in Fig. 10(b), 4 vials containing deionized water, 5 and 100 mg/l of the MB dye, and the dye treated using the heat-treated CBBO glass-ceramic sample for 30 min were used for seed germination experiments. All the experiments regarding seed germinations were performed at 25 °C at IIT Mandi, India. The reduced seed length is related to the toxicity of the water used for germination. Therefore, the seed that germinates after being exposed to the treated water can be used as a safety measure. Using the following equation, we may get the germination index (GI):[47]

$$GI(\%) = \frac{(Seed\ germination(\%)) * (root\ treatment)}{(seed\ germination(\%)) * (root\ length\ of\ control)} * 100. \tag{11}$$

For all of the 5, 100 mg/l, and treated water using the CBBO glass-ceramic samples, the computed measure of phytotoxicity is displayed in Fig. 10(a). There are three levels of phytotoxicity assessed by GI: high (GI < 50%), low (GI > 80%), and medium (80% < GI < 50%). The figure shows that the GI values for 5 and 100 mg/l are 28% and 10%, respectively, whereas the GI value for the treated water is 85%, placing it in the category of reduced phytotoxicity. Changing several factors, such as the MB dye content, catalyst quantity, or catalytic method, should lead to a higher GI value.

After the successful evaluation of the piezocatalytic performance of the CBBO glass-ceramic samples for the degradation of dye, the antibacterial activity was also investigated. The as-prepared (AQ) and heat-treated glass samples for 30 min of CBBO (HT30m) were used along with the control sample. The piezocatalytic activity was used to sterilize water contamination with *S. aureus* (gram-positive) and *E. coli* (gram-negative) bacteria for 120 min. The bacteria were piezocatalytically treated in the control (no sample), AQ, and HT30m samples. After the treatment, the solution containing the bacteria was spread over the LB agar and allowed to
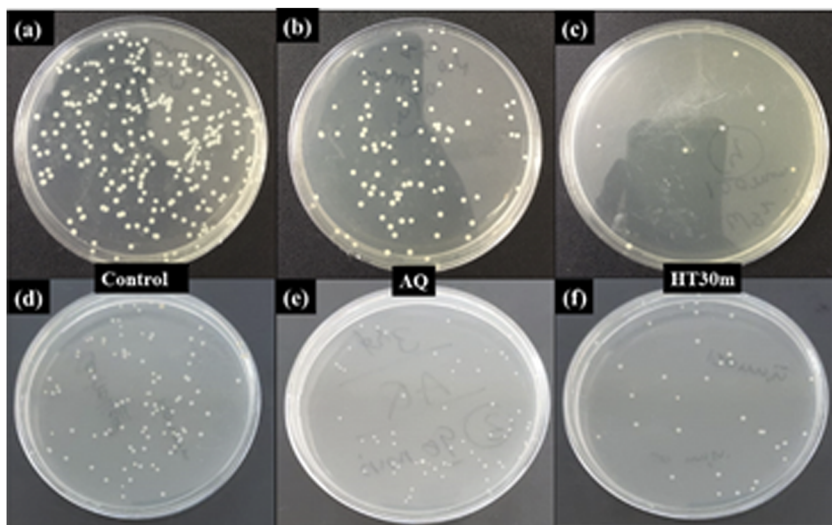

FIG. 11. (a)–(c) Optical images of the antibacterial performance of the control, AQ, and HT30m samples of the CBBO glass-ceramic plate of an *S. aureus* cell colony. (d)–(f) Optical images of the antibacterial performance of the control, AQ, and HT30m samples of the CBBO glass-ceramic plate of an *E. coli* cell colony.
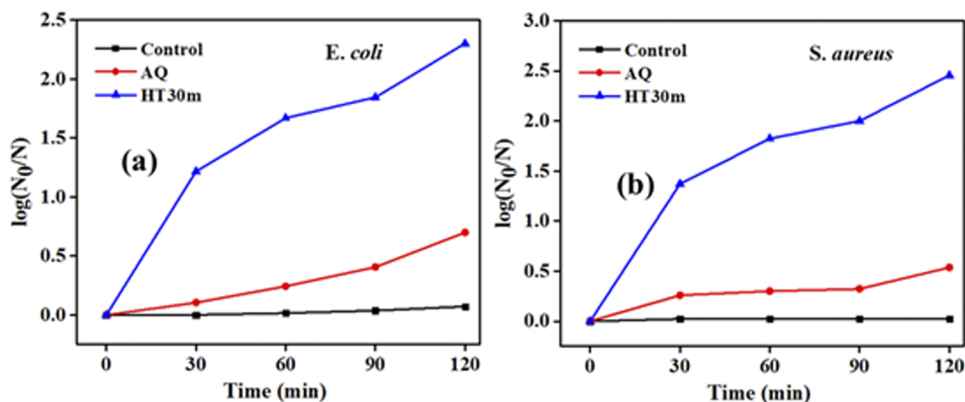
18 April 2024 20:02:34

FIG. 12. (a) and (b) Time-dependent log reduction of CFUs/ml of *E. coli* and *S. aureus* for all the samples under consideration.

grow for 18 h under suitable conditions. As Figs. 11(a)–11(c) show, the number of colonies of the *S. aureus* bacteria had decreased after 120 min of treatment for all three samples under consideration. The same results were obtained in the case of *E. coli* after 120 min of ultrasonic treatment. The photographic images of plating are shown in Figs. 11(d)–11(f). It can be said that the prepared CBBO glass plate with or without heat treatment is an excellent candidate with antibacterial properties. A comparative evaluation has been done for all the samples under consideration and is plotted in the form of log reduction in Figs. 12(a) and 12(b) for the *E. coli* and *S. aureus* bacteria. The obtained results show that the heat-treated sample of the CBBO glass-ceramic for 30 min (HT30m) has a maximum log reduction in the CFUs/ml of bacteria. The possible reason for such a performance may be the generation of reactive oxygen species (ROS) during ultrasonication and the enhancement in the antibacterial performance with the use of the HT30m sample. The mechanism of antibacterial activity is not truly known to date, but it may encompass the formation of ROS that harm the cell membrane. The generation of ROS has been frequently linked to the piezocatalysis and antibacterial activity of many materials.[48]

IV. CONCLUSIONS

In this study, the $CaO–Bi_2O_3–B_2O_3$ (CBBO) transparent glass-ceramic was subjected to heat treatment at $540\,^{\circ}C$ for 30 min and 1 h, resulting in a decrease in transparency and an increase in crystallization. X-ray diffraction (XRD) and Raman analysis were utilized to confirm the phases and their nature in the prepared samples. Scanning electron microscopy (SEM) was used to examine the surface morphology of the CBBO glass-ceramic samples. The CBBO glass-ceramic samples exhibited an excellent piezocatalytic activity for dye degradation, with the heat-treated sample for 30 min at $540\,^{\circ}C$ (HT30m) demonstrating the greatest potential for dye degradation via piezocatalysis. The HT30m CBBO glass-ceramic sample exhibited a dye degradation rate of $0.0045\ min^{-1}$. Moreover, phytotoxicity evaluation experiments were performed on vigna radiata seeds utilizing a byproduct generated from the degraded dye. When using the water treated with the CBBO glass-ceramic sample, the water phytotoxicity was found to be reduced by 85%, as

previously demonstrated in a recent investigation. Furthermore, the antibacterial properties of the CBBO glass-ceramic samples were investigated via piezocatalysis. The HT30m CBBO glass-ceramic sample removed 98% of *Escherichia coli* and 99% of *Staphylococcus aureus* bacteria within 120 min of ultrasonication, highlighting its potential for antibacterial applications.

AUTHOR DECLARATIONS

Conflict of Interest

The authors have no conflicts to disclose.

Author Contributions

Chirag Porwal: Conceptualization (lead); Methodology (lead); Writing – original draft (lead); Writing – review & editing (equal). **Vishal Singh Chauhan**: Methodology (equal); Writing – review & editing (equal). **Rahul Vaish**: Conceptualization (equal); Writing – review & editing (equal).

DATA AVAILABILITY

The data that support the findings of this study are available within the article.

REFERENCES

[1]H. Masai, T. Toda, Y. Takahashi, and T. Fujiwara, Appl. Phys. Lett. **94**, 151910 (2009).
[2]H. Masai, T. Toda, T. Ueno, Y. Takahashi, and T. Fujiwara, Appl. Phys. Lett. **94**, 151908 (2009).
[3]P. Hartmann, K. Nattermann, T. Döhring, R. Jedamzik, M. Kuhr, P. Thomas, G. Kling, and S. Lucarelli, Proc. SPIE **7425**, 74250M (2009).
[4]F. Woodard, *Industrial Waste Treatment Handbook* (Elsevier, 2001).
[5]S. Park and W. Labys, Industrial Development and Environmental Degradation (1998).
[6]C. Porwal, V. S. Chauhan, and R. Vaish, Surf. Interfaces **36**, 102636 (2023).
[7]K. Kabra, R. Chaudhary, and R. L. Sawhney, Ind. Eng. Chem. Res. **43**, 7683 (2004).
[8]K. Nakata and A. Fujishima, J. Photochem. Photobiol., C **13**, 169 (2012).
[9]A. Gaur, M. Sharma, V. S. Chauhan, and R. Vaish, J. Am. Ceram. Soc. **105**, 5140 (2022).

[10]G. Singh, M. Kumar, M. Singh, and R. Vaish, J. Am. Ceram. Soc. **104**, 1237 (2021).

[11]X. Liu, L. Xiao, Y. Zhang, and H. Sun, J. Materiomics **6**, 256 (2020).

[12]B. Yuan, J. Wu, N. Qin, E. Lin, and D. Bao, ACS Appl. Nano Mater. **1**, 5119 (2018).

[13]J. Xu, T. Zang, D. Du, S. Kumar, M. Sharma, and R. Vaish, J. Am. Ceram. Soc. **104**, 1661 (2021).

[14]T. Ida, K. Shinozaki, T. Honma, and T. Komatsu, J. Asian Ceram. Soc. **2**, 253 (2014).

[15]V. P. Singh, H. S. Kushwaha, and R. Vaish, Mater. Res. Bull. **99**, 453 (2018).

[16]S. K. Sharma, V. P. Singh, V. S. Chauhan, H. S. Kushwaha, and R. Vaish, J. Appl. Phys. **122**, 094901 (2017).

[17]J. Fu, Mater. Res. Bull. **46**, 2523 (2011).

[18]K. Wang, C. Han, J. Li, J. Qiu, J. Sunarso, and S. Liu, Angew. Chem. **134**, e202110429 (2022).

[19]G. Singh, M. Sharma, and R. Vaish, Adv. Powder Technol. **31**, 1771 (2020).

[20]G. Singh, M. Sharma, and R. Vaish, Commun. Mater. **1**, 100 (2020).

[21]G. Singh, M. Sharma, and R. Vaish, J. Appl. Phys. **130**, 125101 (2021).

[22]K. Majhi and K. B. R. Varma, J. Mater. Sci. **44**, 385 (2009).

[23]E. R. Shaaban, M. Shapaan, and Y. B. Saddeek, J. Phys.: Condens. Matter **20**, 155108 (2008).

[24]C. Dohare and N. Mehta, J. Cryst. Process Technol. **02**, 167 (2012).

[25]S. Mahadevan, A. Giridhar, and A. K. Singh, J. Non-Cryst. Solids **88**, 11 (1986).

[26]J. Barbier and L. M. D. Cranswick, J. Solid State Chem. **179**, 3958 (2006).

[27]A. V. Vdovin, V. N. Moiseenko, and Y. V. Burak, Opt. Spectrosc. **90**, 555 (2001).

[28]P. M. Rafailov, A. V. Egorysheva, T. I. Milenov, V. D. Volodin, G. V. Avdeev, R. Titorenkova, V. M. Skorikov, R. Petrova, and M. M. Gospodinov, Appl. Phys. B **101**, 185 (2010).

[29]J. F. Stebbins and Z. Xu, Nature **390**, 60 (1997).

[30]H. Li, Y. Zhang, H. Ou, T. Ma, and H. Huang, Colloids Surf., A **584**, 123994 (2020).

[31]S. Singh and K. Singh, J. Non-Cryst. Solids **386**, 100 (2014).

[32]C. Porwal, S. Verma, M. Kumar, V. S. Chauhan, and R. Vaish, Nano-Struct. Nano-Obj. **34**, 100969 (2023).

[33]S. Mansingh, R. Acharya, S. Martha, and K. M. Parida, Phys. Chem. Chem. Phys. **20**, 9872 (2018).

[34]S. Acharya, S. Mansingh, and K. M. Parida, Inorg. Chem. Front. **4**, 1022 (2017).

[35]G. Tezcanli-Güyer and N. H. Ince, Ultrasonics **42**, 603 (2004).

[36]N. Ghows and M. H. Entezari, Ultrason. Sonochem. **20**, 386 (2013).

[37]S. Tu, Y. Guo, Y. Zhang, C. Hu, T. Zhang, T. Ma, and H. Huang, Adv. Funct. Mater. **30**, 2005158 (2020).

[38]J. Yuan, Q. Wu, P. Zhang, J. Yao, T. He, and Y. Cao, Environ. Sci. Technol. **46**(4), 2330 (2012).

[39]J. Liu, W. Zhao, B. Wang, and H. Yan, Chem. Phys. Lett. **728**, 62 (2019).

[40]H. Huang, Y. He, Z. Lin, L. Kang, and Y. Zhang, J. Phys. Chem. C **117**, 22986 (2013).

[41]Y. Li, Y. Diao, X. Wang, X. Tian, Y. Hu, B. Zhang, and D. Yang, Inorg. Chem. **59**, 13136 (2020).

[42]J. Liu, W. Zhao, B. Wang, and H. Yan, J. Mater. Sci.: Mater. Electron. **29**, 13803 (2018).

[43]Y. Zhai, Y. Zhang, J. Yin, and X. Fan, Appl. Surf. Sci. **484**, 981 (2019).

[44]J. Liu, X. Fan, Y. Zhu, J. Zhao, F. Jiang, S. Chen, H. Sun, J. Xu, W. Deng, and C. Wang, Appl. Catal., B **181**, 436 (2016).

[45]C. Porwal, M. Sharma, R. Vaish, V. S. Chauhan, S. b. Ahmed, W. Hwang, H. K. Benno Park, T. H. Sung, and A. Kumar, J. Mater. Res. Technol. **21**, 2028 (2022).

[46]C. Porwal, M. Sharma, R. Vaish, and V. S. Chauhan, ACS Appl. Eng. Mater. **1**, 295 (2022).

[47]S. Verma, M. Sharma, A. Halder, and R. Vaish, Surf. Interfaces **30**, 101827 (2022).

[48]W. He, H.-K. Kim, W. G. Wamer, D. Melka, J. H. Callahan, and J.-J. Yin, J. Am. Chem. Soc. **136**, 750 (2014).

18 April 2024 20:02:34